Cross sections for elastic scattering of electrons by CF3Cl, CF2Cl2, and CFCl3

M. Hoshino, M. Horie, H. Kato, F. Blanco, G. García et al.

Citation: J. Chem. Phys. **138**, 214305 (2013); doi: 10.1063/1.4807610
View online: http://dx.doi.org/10.1063/1.4807610
View Table of Contents: http://jcp.aip.org/resource/1/JCPSA6/v138/i21
Published by the AIP Publishing LLC.

Cross sections for elastic scattering of electrons by CF_3Cl, CF_2Cl_2, and $CFCl_3$

M. Hoshino,[1,a)] M. Horie,[1] H. Kato,[1] F. Blanco,[2] G. García,[3] P. Limão-Vieira,[1,4] J. P. Sullivan,[5] M. J. Brunger,[6,7] and H. Tanaka[1]

[1]*Department of Physics, Sophia University, Chiyoda-ku, Tokyo 102-8554, Japan*
[2]*Departamento de Física Atómica, Molecular y Nuclear, Facultad de Ciencias Físicas, Universidad Complutense de Madrid, E-28040 Madrid, Spain*
[3]*Instituto de Física Fundamental, Consejo Superior de Investigaciones Científicas, 28006 Madrid, Spain*
[4]*CEFITEC, Departamento de Física, Faculdade de Ciências e Tecnologia, Universidade Nova de Lisboa, 2829–516 Caparica, Portugal*
[5]*ARC Centre for Antimatter-Matter Studies, AMPL, Research School of Physics and Engineering, Australian National University, Canberra, ACT 0200, Australia*
[6]*ARC Centre for Antimatter-Matter Studies, CaPS, Flinders University, GPO Box, 2100, Adelaide, SA 5001, Australia*
[7]*Institute of Mathematical Sciences, University of Malaya, Kuala Lumpur 50603, Malaysia*

(Received 18 March 2013; accepted 9 May 2013; published online 4 June 2013)

Differential, integral, and momentum transfer cross sections have been determined for the elastic scattering of electrons from the molecules CF_3Cl, CF_2Cl_2, and $CFCl_3$.With the help of a crossed electron beam–molecular beam apparatus using the relative flow technique, the ratios of the elastic differential cross sections (DCSs) of CF_3Cl, CF_2Cl_2, and $CFCl_3$ to those of He were measured in the energy region from 1.5 to 100 eV and at scattering angles in the range 15° to 130°. From those ratios, the absolute DCSs were determined by utilizing the known DCS of He. For CF_3Cl and CF_2Cl_2, at the common energies of measurement, we find generally good agreement with the results from the independent experiments of Mann and Linder [J. Phys. B **25**, 1621 (1992); **25**, 1633 (1992)]. In addition, as a result of progressively substituting a Cl-atom, undulations in the angular distributions have been found to vary in a largely systematic manner in going from CF_4 to CF_3Cl to CF_2Cl_2 to $CFCl_3$ and to CCl_4. These observed features suggest that the elastic scattering process is, in an independently additive manner, dominated by the atomic-Cl atoms of the molecules. The present independent atom method calculation typically supports the experimental evidence, within the screened additivity rule formulation, for each species and for energies greater than about 10–20 eV. Integral elastic and momentum transfer cross sections were also derived from the measured DCSs, and are compared to the other available theoretical and experimental results. The elastic integral cross sections are also evaluated as a part of their contribution to the total cross section. © *2013 AIP Publishing LLC*. [http://dx.doi.org/10.1063/1.4807610]

I. INTRODUCTION

In studying trends (similarities and differences) of electron scattering from related series of atoms and molecules, one can then try and deduce a simple and intuitively correct interpretation for the underlying species' scattering physics. In our research program at Sophia University for such series of molecules, we have reported absolute differential cross sections (DCSs) for elastic electron scattering from CH_nF_{4-n} (n = 0–4),[1,2] XY_4 (X = C, Si, Ge; Y = H, F, Cl),[3–6] CX_3Y (X = H, F; Y = H, F, Cl, Br, I),[7,8] C_3H_8 and C_3F_8,[9] C_6H_5X ($X = CH_3$, CF_3),[10] and CO_2, OCS, and CS_2.[11,12] Those results have been compared with the corresponding elastic cross sections in Ne, Ar, Kr, and Xe (see, e.g., Ref. 8), F, Cl, Br, and I (see, e.g., Refs. 4, 6, and 8) and S atoms.[13] In comparing these series of molecules, in general, it has been found that "atomic-like" effects prevail in the high-energy electron scattering processes, rather than the underlying molecular structures of the target. Further evidence in support of this feature, of "atomic-like" effects being important in high-energy elastic scattering, can be seen in the excellent agreement with the corresponding independent atom method–screening corrected additivity rule (IAM–SCAR) results.

Previously these typical CFC gases, i.e., the chlorofluoromethanes, of this study, have been considered important due to their nature as an environmental chemical pollutant. However, since their regulation under global treaties (Vienna Convention for the Protection of the Ozone Layer, 1985, and the Montreal Protocol on Substances that Deplete the Ozone Layer, 1987),[14] this is perhaps a less important motivation for their ongoing study. In the present case, we are in fact primarily interested in the fundamental physics and chemistry of these targets.

Although there have been earlier studies of those systems, using the electron-energy-loss technique to experimentally identify their electronic states,[15–17] to the best of our knowledge no complete study based on electron-scattering

a)Author to whom correspondence should be addressed. Electronic mail: masami-h@sophia.ac.jp. Tel.: (+81) 3 3238 4227. Fax: (+81) 3 3238 3341.

elastic differential cross sections (DCSs) has been carried out to date, i.e., an arguably more suitable object for a detailed and accurate study in the wide energy range from a few eV to 100 eV. Elastic and vibrational excitation cross sections for CF_2Cl_2 and CF_3Cl have been reported only by Mann and Linder,[18,19] using the crossed electron–molecular beam geometry in the energy range from 1 to 10 eV and for scattering angles between 10° and 100°. Calculations for those molecules have been performed by Natalense *et al.*[20] and Varella *et al.*,[21] with the Schwinger multichannel (SMC) method in the energy range from 5 eV to 100 eV for CF_3Cl.[2] In addition, but now from 5 eV to 30 eV, they also reported results for CF_2Cl_2 and $CFCl_3$.[2,20,21] Total cross sections for CF_3Cl, CF_2Cl_2, and $CFCl_3$ have been measured by Jones, using a time-of-flight apparatus between 0.5 and 50 eV,[22] by Zecca *et al.* using a Ramsauer-type transmission configuration between 80 eV and 4000 eV,[23] by Underwood-Lemons *et al.* using a trochoidal spectrometer for CF_3Cl and CF_2Cl_2 between 0.2 eV and 12 eV[24] and by Randell *et al.* using a magnetically confined photoelectron sourced from Ar, induced by synchrotron radiation, between energies from less than 10 meV to a few hundred meV.[25]

In this report we present further results from our studies into electron scattering from the chlorofluoromethanes. Specifically, elastic DCSs for energies between 1.5 and 100 eV and for scattering angles in the range 15°–130° are given and discussed. Elastic integral cross sections (ICSs) and momentum transfer cross sections (MTCSs), derived from the present DCS using a modified phase shift analysis (PSA) are also reported. Our previous DCSs for CF_4[26] and CCl_4,[6] with the non-polar T_d symmetry, are also included here in our discussion of the comparative behaviour of the $CF_{4-x}Cl_x$ (x = 0, 1, 2, 3, 4) series of molecules. In Sec. II of this paper we provide a brief description of our experimental apparatus and measurement and analysis procedures, with an outline of our IAM–SCAR calculations being given in Sec. III. After our results and discussion in Sec. IV, some conclusions are finally drawn.

II. EQUIPMENT AND FITTING PROCEDURES

A. Apparatus and operating procedures

The present experimental apparatus and method have been described in detail in earlier papers,[27,28] so that only a brief précis of them is required here. The apparatus consists of an electron-scattering spectrometer, gas flow system, and counting electronics for detecting and storing the scattered electron signal. The scattering spectrometer contains an electron gun and hemispherical monochromator, which produce a nearly monoenergetic electron beam of the desired energy, a detector with a hemispherical energy analyzer, a channeltron for the detection of scattered electrons and a nozzle through which a target gas effuses to produce a well-defined beam of the molecules under study. Both the monochromator and the detector are enclosed in differentially pumped boxes to, respectively, reduce the effect of background gases and to minimize the stray electron background. The electron-optic properties of the multicomponent lens system are carefully calculated with an electron trajectory program (SIMION). For some lens elements the driving voltages are, therefore, controlled by programmable power supplies in order to keep the transmission of the scattered electrons constant. The incident electron beam crosses the molecular beam at right angles and the scattered electrons can be detected in the angular region between 15° and 130°, with respect to the incident electron beam. The spectrometer and the surroundings of the collision region are heated to a temperature of about 60 °C, in order to reduce any possible contamination during the measurements. The gas samples were supplied from the Takachiho Chemical Company with a standard purity better than 99.9%.

During the present measurements, the overall energy resolution of the spectrometer was 35–40 meV, with a few nanoamperes (depending on the initial electron energy) of incident electron flux as measured in a Faraday Cup, and the angular resolution was ±1.5°. With this energy resolution, there could be contributions to the elastic signal from some of the lower lying vibrational modes of the CF_3Cl, CF_2Cl_2, and $CFCl_3$ molecules. However in the energy range above 10 eV, these possible vibrational contributions are expected to be very small compared to the elastic intensity, and thus are not expected to make any significant contribution to the measured elastic cross sections. On the other hand, below 10 eV, possible inelastic contributions have been extracted by deconvoluting the energy loss spectra with Gaussian profiles thus removing them from the elastic DCSs. Figure 1 shows an example of this process for $CFCl_3$. The incident electron (e) energy is calibrated against the 19.365 eV resonance in He,[29] as well as the 1.97 eV vibrational excitation ($\nu' = 0$–1) of the $^2\Pi_g$ resonance in N_2.[30]

The cross-section calibration procedure, the so-called relative flow method,[31,32] was employed in this study. Here the ratio of the elastically scattered intensity of the molecular gas to that of He, under the same experimental conditions, was determined experimentally. Subsequently, employing the known He elastic DCSs,[33] we can derive the present elastic DCSs of CF_3Cl, CF_2Cl_2, and $CFCl_3$. The calibration we employ requires constant Knudsen numbers for equal molecular densities in the collision volume, for which the values of the hard sphere diameters for He (2.18 Å^2) and the molecules of interest (shown in Table I)[34] were used.

B. Fitting and integration methods

In order to compare the present results with the total cross sections reported in literature, elastic integral cross sections (ICSs: Q_I) and momentum transfer cross sections (MTCSs: Q_M) are obtained by integration of the measured DCSs. Note that these integrals are fairly insensitive to detail of the extrapolation tails (i.e., at large and small scattering angles), due to the sine factor in the integrand of the relevant formulae,

$$Q_I(E) = 2\pi \int \mathrm{DCS}(\vartheta) \sin\vartheta \, d\vartheta, \tag{1}$$

$$Q_M(E) = 2\pi \int \mathrm{DCS}(\vartheta)(1 - \cos\vartheta) \sin\vartheta \, d\vartheta. \tag{2}$$

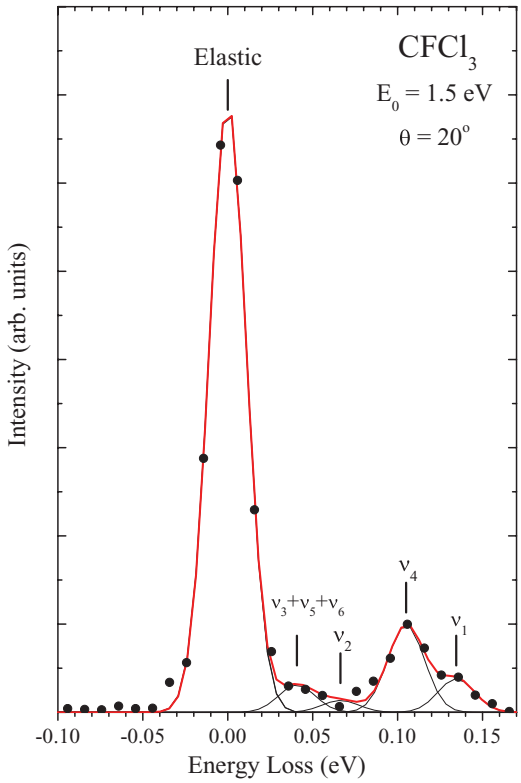

FIG. 1. Typical energy loss spectrum for electron scattering from $CFCl_3$. The elastic peak and low-lying vibrational quanta are denoted, as is our spectral deconvolution of these data. The incident electron energy was 1.5 eV and the scattered electron angle was 20°.

In the present case, the DCSs for $\theta < 15°$ and $\vartheta > 130°$ are extrapolated by using either a modified phase shift analysis (see Eqs. (3)–(5)), including polarization and the Born approximation for the higher phase shifts (see Eq. (5)), or the corresponding shapes of our IAM–SCAR [see Sec. III] calculation and the SMC[2,20,21] calculations as a guide.

Under the modified phase shift analysis described previously,[35] as a supplemental tool for carrying out the integrations, the parameterization of the scattering amplitude $f(\vartheta)$ is defined as follows:

$$\mathrm{DCS}(\vartheta) \equiv \frac{d\sigma_0}{d\theta} = |f(\vartheta)|^2, \tag{3}$$

and

$$2ikf(\vartheta) = N(k)\left\{\sum_{\ell=0}^{L}[S_\ell(k)-1](2\ell+1)P_\ell(\cos\vartheta) + C_L(\vartheta)\right\}, \tag{4}$$

with

$$C_L(\vartheta) = 2i\pi\alpha k^2\left\{\frac{1}{3} - \frac{1}{2}\sin(\vartheta/2) - \sum_{\ell=1}^{L} P_\ell(\cos\vartheta)/(2\ell+3)(2\ell-1)\right\}. \tag{5}$$

Here k is the incident electron wavenumber, S_ℓ is the scattering matrix, and $N(k)$ depends on the least-squares fitting procedure employed. C_L is the Thompson[36] coefficient from the Born approximation for higher order phase shifts beyond a cutoff value L, and α *is* the polarizability of the target. Values of α pertinent to this study can be found in Table I. In the case of the simple phase fitting as used for spherical potentials,[37] $N(k)$ would be unity and $S_\ell = \exp(i\delta_\ell)$. When dealing with only approximately spherical potentials, as in the present case, $N(k)$ becomes an additional size-fitting parameter[38] to be determined together with the phase shifts δ_ℓ. Obviously, this approximation changes the interpretation of the derived phase shifts. With these modifications, Eqs. (3)–(5) have enabled us to obtain excellent fits to experimental data for many different gases (see, for example, Refs. 39–41). Note that the point dipole cross section in the Born approximation—which gives a fairly good approximation for $\theta \leq 10°$—and scales with the square of the dipole moment, is not considered in the present analysis.

As shown in Figs. 2(a)–2(c), the present PSA fitting results typically follow theory in the unaccessed DCS angular regions up to an impact energy of 60 eV. However for $L < 5$, the maximum L being limited by the number of experimental points and the intended degree of smoothing, the factor $N(k)\alpha k^2$ in Eq. (4) overestimates the Born correction at high impact energies. On the other hand, at low energies k^2 makes the fit nearly independent of α. Therefore, above 10 eV, the shape of the IAM–SCAR theory is more reliable to help obtain the integral cross section. This is reasonable as the calculation is in good agreement with the experiment over the range of angles measured for the DCS at these energies, as discussed in more detail in Sec. IV. Furthermore, the SMC method is also sometimes used for interpolation and extrapolation of the experimental DCS data, in cases where the agreement is similarly good between experiment and theory.

We estimate that the overall experimental uncertainties on our elastic DCSs lie in the range of 15%–20%, while the corresponding errors are ∼25% for the ICSs and ∼30% for the MTCSs. It is conceivable that the largest component of the error on the elastic DCSs is due to the uncertainty in the cross

TABLE I. A selection of the important physico-chemical properties of the chlorofluoromethanes considered in this investigation.

Property/molecular species	CF_4	CF_3Cl	CF_2Cl_2	$CFCl_3$	CCl_4
Dipole moment (D)	0	0.5	0.51	0.49	0
Bond length (Å)					
C–F	1.322	1.328	1.342	1.44	…
F–F	2.16	…	…	…	…
C–Cl	…	1.751	1.75	1.76	1.766
Cl–Cl	…	…	…	…	2.887
Bond angle (deg)					
∠F–C–F	109.5	108.6	107.5	…	…
∠F–C–Cl	…	…	109.3	…	…
∠Cl–C–Cl	…	…	112.1	113	109.5
Molecular diameter (Å)	5.3	5.5	5.9	5.7	6.5
Polarizabilities (Å^3)	3.838	5.72	7.93	9.47	10.5
Ionizational potentials (eV)	16.2	12.6	12.05	11.77	11.47
Symmetry	T_d	C_{3v}	C_{2v}	C_{3v}	T_d
GWP (100 year)	7,390	14 400	10 900	4750	1400
Overall lifetime (year)	>50 000	640	100	45	42

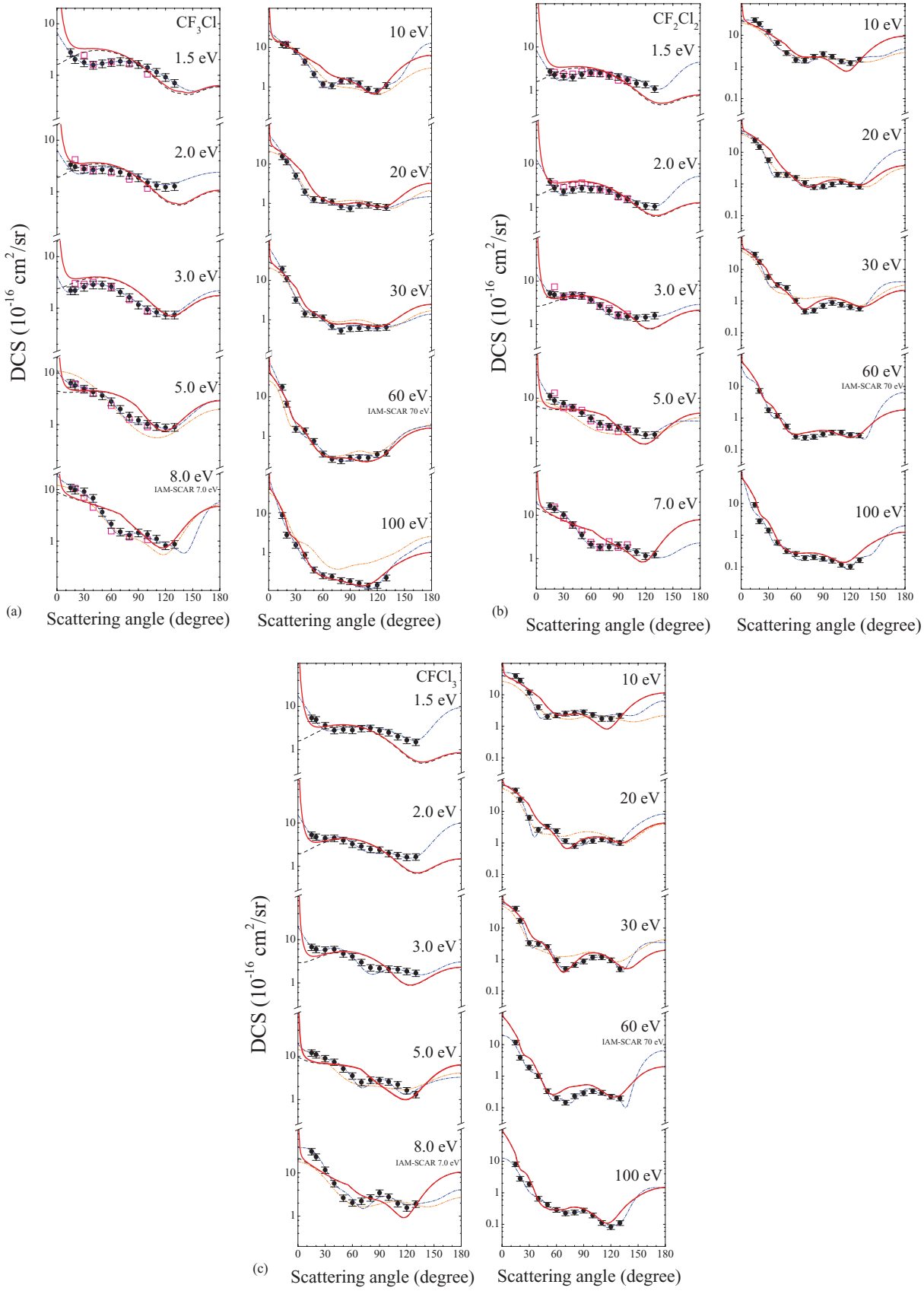

FIG. 2. (a) Present elastic DCSs ($\times 10^{-16}$ cm^2/sr) (●) for electron scattering from CF_3Cl are compared against earlier data from Mann and Linder (□),[18] the present IAM–SCAR calculations with rotations (——) and without rotations (– – –), SMC computational results (- · · · · · -),[20] and the results from our PSA fits (– · – · –). (b) Present elastic DCSs ($\times 10^{-16}$ cm^2/sr) (●) for electron scattering from CF_2Cl_2 are compared against earlier data from Mann and Linder (□),[19] the present IAM–SCAR calculations with rotations (——) and without rotations (– – –), SMC computational results (- · · · · · -),[20] and the results from our PSA fits (– · – · –). (c) Present elastic DCSs ($\times 10^{-16}$ cm^2/sr) (●) for electron scattering from $CFCl_3$ are compared against the present IAM–SCAR calculations with rotations (——) and without rotations (– – –), SMC computational results (- · · · · · -),[20] and the results from our PSA fits (– · – · –).

sections of the helium reference gas (∼10%). The additional error in the values of the ICSs and MTCSs is due to uncertainties associated with the present extrapolation process.

III. THEORETICAL OUTLINE

In order to obtain a better understanding of our experimental results, we have calculated the *e*-CF_3Cl, CF_2Cl_2, and $CFCl_3$ elastic cross sections by using the screening corrected independent atom scattering method (IAM–SCAR) approach. This paradigm has been proven to be a reasonably successful tool for reproducing experimental observations at higher energies, not only for electron-polyatomic molecule collisions (e.g., Refs. 4–6, 8, and 13), but also with electron-diatomic molecules. In particular, the method is useful for studying larger molecules where other *ab initio* theoretical approaches are not readily applicable due to the required extensive computer time. Given the previous discussions of this technique in the literature, a brief description will suffice here for the present purposes.

In the IAM–SCAR approach,[42–46] the first subjects of the present calculations are the atoms constituting the molecules in question, namely, C, F, and Cl. We represent each atomic target by an interacting complex potential (the so-called optical potential), whose real part accounts for the elastic scattering of the incident electrons, while the imaginary part represents the inelastic processes which are considered as "absorption" from the incident beam. To construct this complex potential for each atom, we followed the procedure proposed by Staszewska *et al.*,[47] where the real part of the potential is represented by the sum of three terms: (i) a static term derived from a Hartree–Fock calculation of the atomic charge density distribution,[48] (ii) an exchange term to account for the indistinguishability of the incident and target electrons,[49] and (iii) a polarization term[50] for the long-range interactions which depends on the target polarizability α.[34] The imaginary part then treats inelastic scattering as electron-electron collisions. However, we initially found some important discrepancies with the available experimental atomic scattering data, which were subsequently corrected when a more physical formulation of the absorption potential[42] was introduced. Further improvements to the original formulation,[47] such as the inclusion of screening effects and in the description of the electron's indistinguishability,[43] finally led to a model which provides a quite good approximation for electron-molecule scattering over the very broad energy range of our program.[4–6,8,13]

To calculate the cross sections for electron scattering from molecules, we follow the IAM by applying a coherent addition procedure, commonly known as the additivity rule (AR). In this approach, the molecular scattering amplitude is derived from the sum of all the relevant atomic amplitudes, including the phase coefficients, therefore leading to the DCSs for the molecule in question. ICSs can then be determined by integrating those DCSs. Alternatively, ICSs can also be derived from the relevant atomic ICSs in conjunction with the optical theorem.[43] Unfortunately, in its original form, we found an inherent contradiction between the ICSs derived from these two approaches, which suggested the optical theorem was being violated.[51] We, however, solved this problem by employing a normalization procedure during the computation of the DCSs, so that ICSs derived from the two approaches are now entirely consistent.[51] A limitation with the AR is that no molecular structure is considered, so that it is really only applicable when the incident electrons are so fast that they effectively only see the target molecule as a sum of the individual atoms (typically when above about 100 eV). To reduce the effect of that limitation, we introduced the SCAR method,[44,45] which considers the geometry of the relevant molecule (atomic positions and bond lengths) by employing some screening coefficients. With this correction the range of validity can be extended to incident electron energies as low as about 20–30 eV. As noted above, for intermediate and high energies, this method has proven to be a powerful tool to calculate electron scattering cross sections from a large variety of molecules of very different sizes, from diatomics to complex biomolecules.[52] Moreover, this approach seems to be inherently suitable for electron scattering from a heavy-atom electron-rich molecule, such as GeF_4, in which its application ranges down to ∼7 eV.[4] Furthermore, e.g., for the polar molecule OCS,[13] additional dipole-excitation cross sections can be calculated through the IAM–SCAR and rotational contribution method,[46,53] which has been successfully used for other polar molecules such as H_2O.[54] Thus, the range of validity of our approach may even be extended to energies possibly below 10 eV.

In the present application, all model improvements described above have been implemented in our DCS and ICS computations, for all species, at each energy considered. We note, however, that the present calculations revealed that contributions from the dipole moment, such as we found previously with OCS,[13] are only significant for scattered electron angles below 10°, which were not experimentally accessed in the present measurements. Importantly, the shaper of those calculations were nonetheless sometimes used to help us obtain the elastic ICS in our extrapolation procedure.

IV. RESULTS AND DISCUSSION

In Table I, we summarize some of the important physicochemical information for each of the CF_4, CF_3Cl, CF_2Cl_2, $CFCl_3$, and CCl_4 molecules required for the discussion that follows. Tables II–IV specifically give the present measured DCSs, and the derived ICSs and MTCSs, for elastic electron scattering from CF_3Cl, CF_2Cl_2, and $CFCl_3$, respectively. Figures 2(a)–2(c), on the other hand, illustrate the angular distributions of the current DCSs for CF_3Cl, CF_2Cl_2, and $CFCl_3$. Also plotted in Figs. 2(a)–2(c), are the corresponding results from our IAM–SCAR computations, the results from our modified phase shift analysis fits to the present DCSs and results from the calculations using the SMC method.[2,20,21] For the CF_3Cl and CF_2Cl_2 molecules, results from the earlier measurements of Mann and Linder[18,19] are also shown. Figure 3 illustrates the substitution effects as you progressively replace a F-atom with a Cl-atom in the series $CF_{4-x}Cl_x$ (x = 0, 1, 2, 3, 4). Note that the data for CF_4 and CCl_4 were reported previously by our group[1,6] and are included here simply for comparison with the present results. For

TABLE II. Present elastic DCSs ($\times 10^{-16}$ cm^2/sr) for electron scattering from CF_3Cl. The current ICSs and MTCSs (both in units of 10^{-16} cm^2), derived from our DCSs, are given at the foot of the table.

	Energy (eV)									
Angle (deg)	1.5	2.0	3.0	5.0	8.0	10	20	30	60	100
15	2.791	3.332	2.214	6.384	10.85	11.97	15.48	19.46	17.68	8.885
20	2.042	3.077	2.202	5.772	9.915	11.51	11.42	11.16	6.623	2.828
30	1.768	2.782	2.874	4.938	9.100	8.114	5.030	3.198	1.527	1.562
40	1.582	2.651	2.858	4.300	6.823	4.344	1.949	1.416	1.378	0.869
50	1.691	2.706	2.846	3.677	3.649	2.100	1.266	1.370	0.751	0.370
60	1.788	2.628	2.610	2.817	2.141	1.168	1.218	1.131	0.357	0.263
70	1.872	2.398	2.045	1.999	1.513	1.081	1.092	0.687	0.262	0.245
80	1.816	2.140	1.625	1.479	1.311	1.437	0.833	0.528	0.242	0.198
90	1.644	1.887	1.166	1.213	1.456	1.449	0.749	0.606	0.283	0.186
100	1.409	1.511	0.946	1.031	1.347	1.213	0.907	0.614	0.290	0.167
110	1.155	1.328	0.831	0.932	1.102	0.871	0.923	0.636	0.284	0.144
120	0.919	1.229	0.748	0.876	0.821	0.784	0.839	0.633	0.345	0.151
130	0.706	1.276	0.748	0.895	0.871	1.102	0.802	0.653	0.378	0.231
ICS	17.62	27.12	20.70	26.82	31.15	32.79	25.30	22.15	16.10	10.56
MTCS	13.98	23.93	16.27	18.17	18.02	24.56	12.68	10.05	7.410	5.160

TABLE III. Present elastic DCSs ($\times 10^{-16}$ cm^2/sr) for electron scattering from CF_2Cl_2. The current ICSs and MTCSs (both in units of 10^{-16} cm^2), derived from our DCSs, are given at the foot of each table.

Angle	Energy (eV)							
(deg)	1.5	2.0	2.6	3.0	4.0	5.0	6.0	7.0
15	2.691	3.942	5.105	5.136	6.594	10.98	15.01	16.48
20	2.290	2.797	5.129	4.839	6.355	8.769	14.15	13.91
30	2.103	2.291	5.115	4.562	5.331	7.558	8.819	10.96
40	1.999	2.565	5.217	4.752	4.543	6.178	6.382	6.051
50	2.284	2.741	4.808	4.617	4.243	4.591	4.272	3.496
60	2.519	2.600	3.870	3.725	3.283	3.456	2.674	2.140
70	2.493	2.590	3.764	2.714	2.438	2.605	2.142	1.843
80	2.175	2.434	2.965	2.077	2.080	2.239	1.975	1.846
90	2.067	1.859	2.042	1.642	1.694	2.106	1.878	2.063
100	1.748	1.545	2.039	1.525	1.702	1.934	1.820	1.775
110	1.446	1.210	1.885	1.418	1.597	1.744	1.573	1.436
120	1.378	1.087	1.644	1.461	1.522	1.426	1.258	1.155
130	1.084	1.056	1.654	1.625	1.346	1.447	1.261	1.265
ICS	27.16	27.92	35.66	32.39	33.92	40.86	39.43	37.41
MTCS	25.05	24.76	26.79	24.19	25.75	28.52	25.23	21.50

Angle	Energy (eV)						
(deg)	8.0	9.0	10	20	30	60	100
15	20.55	24.40	30.30	23.94	29.48	...	9.162
20	16.52	20.35	23.00	14.84	17.42	7.335	2.784
30	10.70	11.43	13.00	5.703	5.848	1.799	1.430
40	5.591	5.849	5.823	1.987	3.256	1.202	0.594
50	2.952	2.739	2.776	1.950	2.641	0.550	0.317
60	1.846	1.450	1.667	1.569	1.034	0.265	0.259
70	1.797	1.535	1.603	1.088	0.470	0.244	0.193
80	2.178	2.087	2.118	0.807	0.508	0.260	0.203
90	2.414	2.286	2.575	0.851	0.715	0.313	0.183
100	2.182	1.998	2.128	0.988	0.886	0.353	0.159
110	1.499	1.374	1.517	1.185	0.776	0.354	0.119
120	1.315	1.193	1.336	0.979	0.651	0.295	0.102
130	1.596	1.517	1.724	0.836	0.586	0.287	0.164
ICS	42.10	41.41	42.94	34.71	30.57	15.17	8.35
MTCS	27.27	25.77	25.41	26.03	15.74	10.18	3.85

TABLE IV. Present elastic DCSs ($\times 10^{-16}$ cm^2/sr) for electron scattering from $CFCl_3$. The current ICSs and MTCSs (both in units of 10^{-16} cm^2), derived from our DCSs, are given at the foot of each table.

Angle	Energy (eV)						
(deg)	1.5	1.8	2.0	3.0	4.0	5.0	6.0
15	5.388	5.231	5.197	5.314	6.734	9.137	12.04
20	4.958	4.390	4.385	4.781	6.011	7.830	10.93
30	3.641	3.652	3.625	4.445	5.809	8.461	8.940
40	2.793	3.136	3.147	4.487	5.968	8.232	7.377
50	2.926	2.951	2.952	3.999	4.734	6.156	5.159
60	2.825	2.694	2.664	3.283	4.087	4.702	3.545
70	3.113	2.595	2.598	2.909	2.992	3.318	2.507
80	3.155	2.327	2.291	2.489	2.256	2.817	2.836
90	2.743	2.053	2.060	2.403	2.153	2.474	2.782
100	2.493	1.901	1.890	2.002	2.105	2.762	2.580
110	2.011	1.650	1.665	1.795	2.050	2.667	2.219
120	1.655	1.445	1.352	1.628	1.857	2.191	1.624
130	1.505	1.443	1.424	1.663	1.693	1.554	1.319
ICS	39.79	38.55	38.14	37.57	44.80	44.29	51.86
MTCS	38.17	39.38	35.00	27.17	29.95	30.41	34.69

Angle	Energy (eV)					
(deg)	8.0	10	20	30	60	100
15	31.30	39.75	46.38	41.67	11.78	8.111
20	23.49	28.46	23.77	17.09	3.895	2.822
30	11.67	11.99	6.329	3.337	1.906	1.884
40	5.729	4.057	2.618	3.161	1.027	0.654
50	2.635	2.037	3.320	2.528	0.339	0.425
60	2.046	2.244	2.404	0.964	0.202	0.291
70	2.239	2.554	1.157	0.510	0.147	0.226
80	2.668	2.690	0.813	0.682	0.235	0.240
90	3.451	2.824	1.140	0.880	0.292	0.278
100	2.791	2.320	1.077	1.174	0.339	0.193
110	1.958	1.732	1.322	1.200	0.304	0.112
120	1.562	1.739	1.213	0.962	0.226	0.083
130	1.919	2.171	1.009	0.500	0.200	0.111
ICS	54.22	55.88	45.61	34.17	11.99	7.660
MTCS	30.97	33.82	26.31	16.74	9.160	4.670

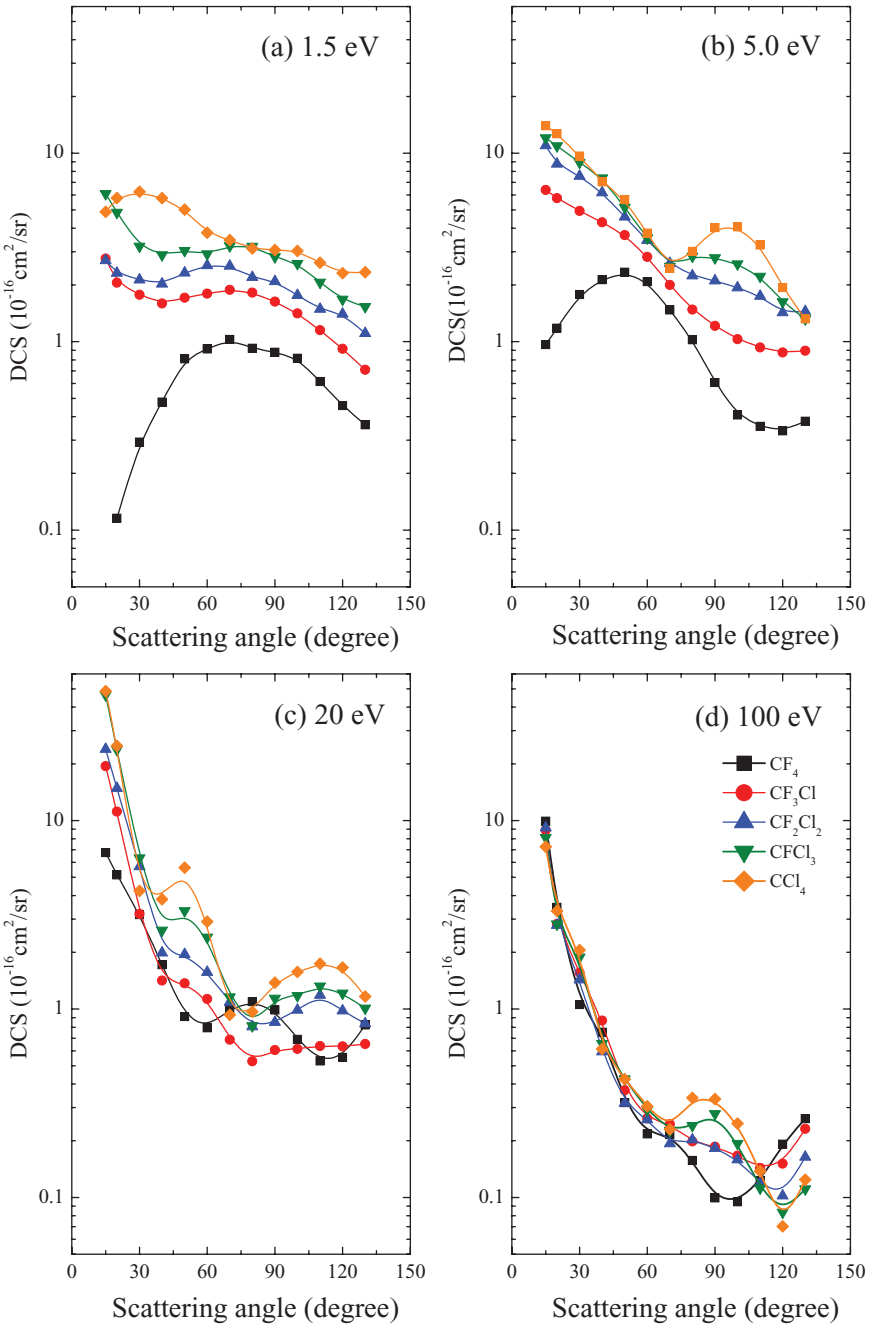

FIG. 3. A comprehensive comparison between the elastic DCSs for the $CF_{4-x}Cl_x$ (x = 0, 1, 2, 3, 4) molecular series. Data at representative incident energies of (a) 1.5 eV, (b) 5 eV, (c) 20 eV, and (d) 100 eV are shown. See also the legend on the panels for more details.

each of the present molecules, our experimental and theoretical elastic ICSs are plotted in Figs. 4(a)–4(c) where they are compared (where possible) with the corresponding results from Mann and Linder.[18,19] Also included in these figures are the available experimental and theoretical total cross sections,[22–25,55–57] elastic ICSs using the SMC approach,[20] and experimental[58–62,64] and BEB theoretical[63] ionization cross sections. The latter cross sections are included for the purpose of sensibly trying to compare our elastic ICS to the available total cross sections. A similar comparison is made in Figs. 5(a)–5(c) for the momentum transfer cross sections. However, there we are limited to comparing the present derived MTCSs to theoretical SMC results.[20]

A. Elastic DCSs

The first systematic data for electron scattering from CF_3Cl, CF_2Cl_2, and $CFCl_3$ are presented in each case over the wide range of energies from 1.5 to 100 eV, and over the scattering angle range between 15° and 130°. This is shown in Figs. 2(a)–2(c). The present results confirm well the DCSs measured by Mann and Linder[18,19] between 1 and 10 eV, to within the error bars, for both CF_3Cl and CF_2Cl_2. Note that the absolute scale in the work of Mann and Linder was defined by normalization to the TCS value of Jones[22] at 4 eV and cross checked further by using the relative-flow technique. Furthermore, our IAM–SCAR calculations agree quite well with the measured DCSs, particularly at impact energies

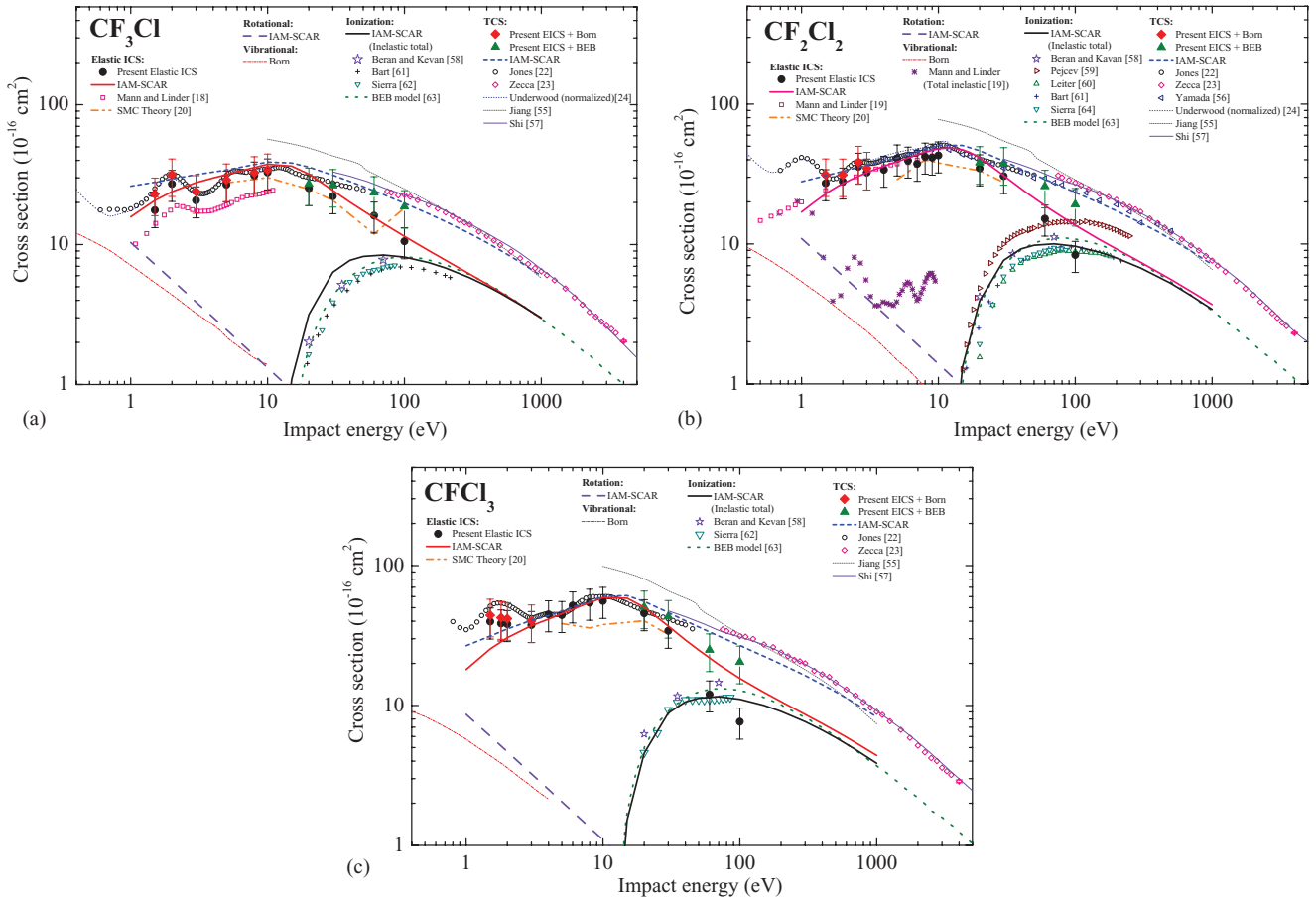

FIG. 4. (a) Present CF_3Cl elastic ICS (●), present ICS plus Born rotational (– – –) and vibrational (– · – · –) terms (◆), and present ICS plus BEB ionization terms (▲) are compared against our elastic IAM-SCAR ICS (——), our total IAM–SCAR cross sections (-----) and our IAM–SCAR ICS for all inelastic processes (——). Also shown are elastic ICS, both theory and experiment, total cross sections and ionization cross sections from other groups. See legend in figure for further details. (b) Present CF_2Cl_2 elastic ICS (●), present ICS plus Born rotational (– – –) and vibrational (– · – · –) terms (◆), and present ICS plus BEB ionization terms (▲) are compared against our elastic IAM–SCAR ICS (——), our total IAM–SCAR cross sections (-----) and our IAM–SCAR ICS for all inelastic processes (——). Also shown are theoretical and experimental elastic ICS, total cross sections and ionization cross sections from other groups. See legend in figure for further details. (c) Present $CFCl_3$ elastic ICS (●), present ICS plus Born rotational (– – –) and vibrational (– · – · –) terms (◆), and present ICS plus BEB ionization terms (▲) are compared against our elastic IAM–SCAR ICS (——), our total IAM–SCAR cross sections (-----) and our IAM–SCAR ICS for all inelastic processes (——). Also shown are theoretical and experimental elastic ICS, total cross sections and ionization cross sections from other groups. See legend in figure for further details.

$\geq$30 eV. The present results are also well described by the SMC calculation below about 8–10 eV, but deviated from the SMC above 20 eV. Though, at lower impact energies <15 eV, all three molecules exhibit resonance phenomena in the TCSs between 1 eV and 15 eV, as shown in Figs. 4(a)–4(c), such characteristics are, in general, expected to be predominantly in the vibrational excitation channels. Indeed one can barely observe them in the elastic scattering channel due to the direct scattering contribution dominating the resonant one. In Fig. 1, for $CFCl_3$ at 1.5 eV and $\theta = 20^\circ$, the energy loss spectrum shows an example in which the vibrational excitations (ν_1–ν_6), are shown with an efficient enhancement of the ν_4 mode (about 15% of the elastic peak) being apparent. In general vibrational excitation is emerging in such resonant energy regions, as well as near an elastic cross section minimum, like the Ramsauer-Townsend effect.[26] Mann and Linder[18,19] observed resonances in their measured vibrational data at 1.7 eV, 5.5 eV, and 8.5 eV for CF_3Cl and at 1.0 eV, 2.5 eV, 4 eV, and 6 eV for CF_2Cl_2. However, the present elastic DCSs (see Figs. 2(a) and 2(b)) show no specific angular features that might be related to those resonant energies. Disregarding any possible resonant effects, it is in fact found that all our DCSs for each target, from direct elastic scattering, reveal very smooth undulations in the angular distributions as the impact energy changes. It is clearly seen that both the local maxima and the minima in all the DCS are growing or disappearing and shifting consistently as the impact energy changes. At the higher impact energies above 10 eV, all the DCS show a strongly forward peaked scattering. We believe that such an angular behaviour is consistent with each of the present three targets having moderate strength dipole moments and dipole polarisabilities (see Table I). Given that direct scattering (compared to resonant scattering) appears to dominate here, the present DCSs indicate that such smooth and distinctive angular behaviours are related to specific angular momenta and probably reflect, at least in part, scattering from the atomic-like target. The systematic deviations of the shoulder emerging around 30° at 5–10 eV in Figure 2(a) may be attributed to a sharp drop of the DCS of CF_4 as shown in Figure 3(a); i.e., although one of F-atoms is replaced by a

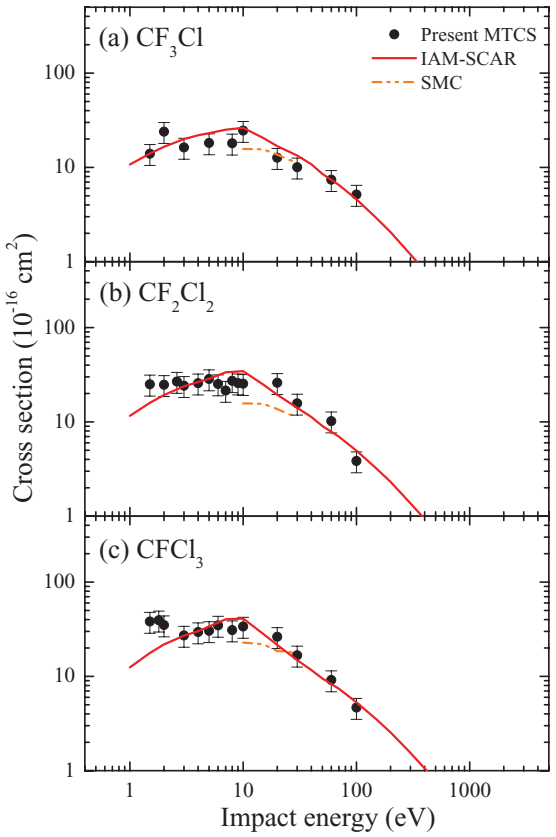

FIG. 5. Present MTCSs ($\times 10^{-16}$ cm^2) (●) for (a) CF_3Cl, (b) CF_2Cl_2, and (c) $CFCl_3$ are compared to the corresponding SMC results (– - - –).[20]

Cl -atom, there are still three F of CF_3 in CF_3 Cl and thus the decreasing trend may still remain around 30° more than for the other two molecules. As we discuss in more detail in Sec. IV B, it is the atomic form factor due to the Cl-atom that dominates the elastic scattering process in these molecules. Finally, we note that it is clear from Figs. 2(a)–2(c) that our modified phase shift analysis fits well to the present DCSs over the wide range of energy from 1.5 to 100 eV and for each target species.

B. Substitution effects of Cl

In order to clarify the effect of progressively substituting atomic-Cl in these molecules, the DCSs measured in this paper, along with those for CF_4[1] and CCl_4,[6] will be discussed in detail for energies of 1.5, 5, 20, and 100 eV. These data are shown in Fig. 3. Here the molecules are initially divided into two groups for later discussion: (i) one for CF_4 and CCl_4, the nonpolar molecules in the series; and (ii) another group for CF_3Cl, CF_2Cl_2, and $CFCl_3$, the polar molecules in the series. Typical features in the present results are summarized as follows. At 1.5 eV the DCSs for class (i) show a decreasing trend in magnitude toward smaller scattering angles <70° for CF_4 and <30° for CCl_4, while those DCSs for class (ii), the partially Cl-substituted (polar) molecules, rapidly continue to grow in magnitude at the smaller scattering angles after the shallow minima at around 40°. This results in a strongly forward peaked angular distribution, a typical characteristic due to the long-range dipole interaction in polar molecules. More precisely, as the number of Cl-atoms increases the cross section minimum at around 40° shifts toward larger angles, and the broad shoulder at around 80° is "pushed out" to larger angles. In addition, as the number of the Cl atoms increases, an increasing trend is revealed systematically in the magnitude of their DCSs. Thus, typically, at any given θ the cross section with the largest magnitude belongs to the CCl_4 target. Although this substitution effect was seen earlier for the series CH_3F, CH_2F_2, and CHF_3 at 1.5 eV, in that case all three DCSs showed their magnitude monotonically increasing toward the smaller scattering angles but with nearly equal magnitudes. The present results thus indicate the strong "atomic-like" scattering dominated by the Cl atom. For our results at 5 eV (see Fig. 3), and with the exception of CF_4, the sharp forward peaking in their DCSs is growing at small scattering angles below 60°, relative to what we saw at 1.5 eV. In addition, particularly for $CFCl_3$ and CCl_4, new secondary maxima are appearing at around 90°. The stark difference between the angular distributions when Cl is present compared to when it is absent (CF_4), indicates that the scattering features for all four Cl-containing molecules are related to the same angular momentum component that dominates in the CCl_4 case. At 20 eV (again see Fig. 3), as the impact energy increases still further, the interaction time between electrons and their molecules, in general, is getting shorter. This roughly corresponds to the direct scattering process with the molecules becoming relatively more important, and thus forward peaking dominates in their DCSs. Of additional note is that with increasing Cl substitution, a secondary maximum in the angular distribution develops at around 50°. Furthermore, a new secondary maximum in the DCS is seen to develop with increasing Cl-atom substitution. It is worth highlighting at 20 eV the very different CF_4 angular distribution compared to those where one or more Cl-atoms have been substituted. Finally, at 100 eV, and for scattering angles less than about 60°, all five DCSs are merging into a single forward peaking function within the error bars. The first secondary maximum seen at 20 eV and 50° has now disappeared and the second local maximum has shifted to ∼90°.

From all of the data presented in Fig. 3, we can surmise that it is the DCSs of atomic Cl that are dominating the elastic electron scattering from the chlorofluoromethanes. Furthermore, the level of agreement with our IAM–SCAR results, as shown in Figs. 2(a)–2(c), supports this idea based on the additivity characteristics for the elastic scattering from molecules.

C. Integral and momentum cross sections

In Figs. 4(a)–4(c) we present our integral elastic cross sections, for CF_3Cl, CF_2Cl_2, and $CFCl_3$, respectively, as derived from our measured DCS in the manner outlined in Sec. II B. Also shown are those ICS when, at the lower energies, results from Born rotational and vibrational integral cross sections are added to them and, at higher energies, results from BEB ionization calculations[63] have been added to them. This was undertaken in order to compare the present results to independent measurements and calculations of the

total cross section for each species.[22–24,55–57] In addition, the results from the present IAM–SCAR calculations for the elastic ICS, total cross sections and sum over all inelastic ICS (except vibrational excitations) are also plotted. Note that independent ionization cross sections[58–64] are also shown for each species, where applicable, to illustrate the efficacy of the BEB model approach. In Figs. 4(a) and 4(b) we compare the present elastic ICS to corresponding results from Mann and Linder,[18,19] where the energy ranges of the two sets of data overlap. Generally, good agreement is found between the results from both groups, to within the error limits of their measurements. Note the discrepancy of the elastic ICSs between Mann and Linder's and the present work shown in Figure 4(a) are due to the extrapolation methods and the normalization procedure. Comparison between the present data and an earlier SMC computation,[20] now for all three targets, also finds satisfactory agreement between them. Similarly, rather good accord is found between our measured ICS and calculated IAM–SCAR elastic ICS for each target, with the exception of the higher energy ICS in CF_2Cl_2 (see Fig. 4(b)) and CF_3Cl (see Fig. 4(c)). If we now add the Born rotational and vibrational ICS, and the BEB ionization[63] ICS, to our elastic ICS we find typically very good agreement between the present "experimental" total cross sections and independent measured TCS from Jones,[22] Zecca *et al.*,[23] and Yamada *et al.*[56] (as appropriate for each target molecule). This is clearly visible in Figs. 4(a)–4(c). Similarly, the present "experimental" TCS are, to within our stated uncertainties, generally found to be in very good agreement with our calculated IAM–SCAR TCS for each target. This important self-consistency test at the total cross section level gives us some confidence in the validity of our DCS measurements and the elastic ICS we have derived from them. Note that given the rather coarse energy grid of our measurements, we typically do not reproduce (except perhaps for CF_3Cl, in Fig. 4(a)) the rich resonance structure observed by Jones.[22]

Finally, in Fig. 5, we present the current MTCSs where a comparison can only be made with our IAM–SCAR theory results and the SMC results.[20] Except perhaps at the lowest energies of our study, typically fair accord is found between our present experimental MTCSs and IAM–SCAR results. Fair agreement was also found between our measured MTCS data and the SMC results,[26] over the more limited energy range where such a comparison was possible. It would be highly desirable if MTCS for these targets were to be determined by independent measurements from, e.g., swarm experiments.

V. CONCLUSIONS

We have reported absolute elastic DCSs for electron scattering from CF_3Cl, CF_2Cl_2, and $CFCl_3$ in the energy range of 1.5–100 eV and over the scattering angles from 15° to 130°. Corresponding theoretical cross sections, calculated by the IAM–SCAR approach as a part of this study, were found to be in good agreement with the experimental data above about 30 eV. The effect of progressively substituting Cl atoms into CF_4 has been reflected systematically in their angular distributions, suggesting that the DCSs of atomic-Cl were dominating the elastic electron scattering process in those systems. Integral elastic cross sections were also determined and found to be largely consistent with the results from the available earlier data, our IAM–SCAR computations and SMC-level results. These elastic ICS were also found to be nicely consistent with the previous results from TCS measurements of other groups (e.g., Refs. 22 and 23), as well as our own IAM–SCAR results. Finally, we note the present MTCSs were, typically, found to be in quite fair accord with both our IAM–SCAR results and the earlier SMC[20] calculations.

ACKNOWLEDGMENTS

The present work has been conducted under the support by the Japanese Ministry of Education, Sport, Culture, and Technology and supported in part by the Australian Research Council through its Centres of Excellence Program. F.B. and G.G. acknowledge partial financial support from the Spanish Ministerio de Economica y Competitividad through Project No. FIS2009-10245, as well as the EU/ESF COST Action MP1002. M.J.B. thanks the JSPS for the provision of a short-term Fellowship and the University of Malaya for a Visiting Professorship. P.L.-V. acknowledges his Visiting Professor position at Sophia University and also the Portuguese PEst-OE/FIS/UI0068/2011 grant. We all thank Dr. L. Campbell for his assistance with some aspects of the production of this paper.

[1] H. Tanaka, T. Masai, M. Kimura, T. Nishimura, and Y. Itikawa, Phys. Rev. A **56**, R3338 (1997).
[2] M. T. do N. Varella, C. Winsted, V. McKoy, M. Kitajima, and H. Tanaka, Phys. Rev. A **65**, 022702 (2002).
[3] M. A. Dillon, L. Boesten, H. Tanaka, M. Kimura, and H. Sato, J. Phys. B **26**, 3147 (1993).
[4] H. Kato, A. Suga, M. Hoshino, F. Blanco, G. Garcia, P. Limao-Vieira, M. J. Brunger, and H. Tanaka, J. Chem. Phys. **136**, 134313 (2012).
[5] H. Kato, K. Anzai, T. Ishihara, M. Hoshino, F. Blanco, G. Garcia, P. Limao-Vieira, M. J. Brunger, S. J. Buckman, and H. Tanaka, J. Phys. B **45**, 095204 (2012).
[6] P. Limão-Vieira, M. Horie, H. Kato, M. Hoshino, F. Blanco, G. García, S. J. Buckman, and H. Tanaka, J. Chem. Phys. **135**, 234309 (2011).
[7] M. Kitajima, M. Okamoto, K. Sunohara, H. Tanaka, H. Cho, H. Samukawa, S. Eden, and N. J. Mason, J. Phys. B **35**, 3257 (2002).
[8] H. Kato, T. Asahina, H. Masui, M. Hoshino, H. Tanaka, H. Cho, O. Ingolfsson, F. Blanco, G. Garcia, S. J. Buckman, and M. J. Brunger, J. Chem. Phys. **132**, 074309 (2010).
[9] H. Tanaka, Y. Tachibana, M. Kitajima, O. Sueoka, H. Takagi, A. Hamada, and M. Kimura, Phys. Rev. A **59**, 2006 (1999).
[10] H. Kato, M. C. Garcia, T. Asahina, M. Hoshino, C. Makochekanwa, H. Tanaka, F. Blanco, and G. Garcia, Phys. Rev. A **79**, 062703 (2009).
[11] O. Sueoka, H. Hamada, M. Kimura, H. Tanaka, and M. Kitajima, J. Chem. Phys. **111**, 245 (1999).
[12] M. Hoshino, A. Suga, H. Kato, F. Blanco, G. García, P. Limão-Vieira, M. J. Brunger, and H. Tanaka, "Absolute elastic and vibrational cross sections for BF_3 by 1.5–200 eV electron impact," J. Chem. Phys. (to be published).
[13] H. Murai, Y. Ishijima, T. Mitsumara, Y. Sakamoto, H. Kato, M. Hoshino, F. Blanco, G. García, P. Limão-Vieira, M. J. Brunger, S. J. Buckman, and H. Tanaka, J. Chem. Phys. **138**, 054302 (2013).
[14] See http://ozone.unep.org/new_site/en/index for the panel assessment on ozone depletion.
[15] G. J. Verhaart, W. J. Van Der Hart, and H. H. Brongersma, Chem. Phys. **34**, 161 (1978).
[16] G. C. King and J. W. McConkey, J. Phys. B **11**, 1861 (1978).
[17] W. Zhang, G. Cooper, T. Ibuki, and C. E. Brion, Chem. Phys. **151**, 343 (1991); **151**, 357 (1991); **153**, 491 (1991); W. Zhang, T. Ibuki, and C. E. Brion, *ibid.* **160**, 435 (1992).
[18] A. Mann and F. Linder, J. Phys. B **25**, 1621 (1992).

[19]A. Mann and F. Linder, J. Phys. B **25**, 1633 (1992).
[20]A. P. P. Natalense, M. H. F. Bettega, L. G. Ferreira, and M. A. P. Lima, Phys. Rev. A **59**, 879 (1999).
[21]M. T. do N. Varella, A. P. P. Natalense, M. H. F. Bettega, and M. A. P. Lima, Phys. Rev. A **60**, 3684 (1999).
[22]R. K. Jones, J. Chem. Phys. **84**, 813 (1986).
[23]A. Zecca, G. P. Karwasz, and R. S. Brusa, Phys. Rev. A **46**, 3877 (1992).
[24]T. Underwood-Lemones, D. C. Winkler, J. A. Tossell, and J. H. Moore, J. Chem. Phys. **100**, 9117 (1994).
[25]J. Randell, J.-P. Ziesel, S. L. Lunt, G. Mrotzerk, and D. Field, J. Phys. B **26**, 3423 (1993).
[26]L. Boesten, H. Tanaka, A. Kobayashi, M. A. Dillon, and M. Kimura, J. Phys. B **25**, 1607 (1992).
[27]H. Tanaka, L. Boesten, D. Matsunaga, and T. Kudo, J. Phys. B **21**, 1255 (1988).
[28]H. Tanaka, T. Ishikawa, T. Masai, T. Sagara, L. Boesten, M. Takekawa, Y. Itikawa, and M. Kimura, Phys. Rev. A **57**, 1798 (1998).
[29]J. N. H. Brunt, G. C. King, and F. H. Read, J. Phys. B **10**, 1289 (1977).
[30]S. F. Wong and L. Dube, Phys. Rev. A **17**, 570 (1978).
[31]S. K. Srivastava, A. Chutjian, and S. Trajmar, J. Chem. Phys. **63**, 2659 (1975).
[32]J. Nickel, P. W. Zetner, G. Shen, and S. Trajmar, J. Phys. E **22**, 730 (1989).
[33]L. Boesten and H. Tanaka, At. Data Nucl. Data Tables **52**, 25 (1992).
[34]*CRC Handbook of Chemistry and Physics*, 88th ed., edited by D. R. Lide (CRC, Boca Raton, FL, 2007).
[35]L. Boesten and H. Tanaka, J. Phys. B **24**, 821 (1991).
[36]D. G. Thompson, Proc. R. Soc. London, Ser. A **294**, 160 (1966).
[37]D. Andrick and A. Bitsch, J. Phys. B **8**, 393 (1975).
[38]D. F. Resister, S. Trajmar, and S. K. Srivastava, Phys. Rev. A **21**, 1134 (1980).
[39]L. Boesten and H. Tanaka, J. Phys. B **24**, 821 (1991).
[40]T. Takagi, L. Boesten, H. Tanaka, and M. A. Dillon, J. Phys. B **27**, 5389 (1994).
[41]L. Boesten, Y. Tachibana, Y. Nakano, T. Shinohara, H. Tanaka, and M. A. Dillon, J. Phys. B **29**, 5475 (1996).
[42]F. Blanco and G. Garcia, Phys. Lett. A **295**, 178 (2002).
[43]F. Blanco and G. Garcia, Phys. Rev. A **67**, 022701 (2003).
[44]F. Blanco and G. Garcia, Phys. Lett. A **317**, 458 (2003).
[45]F. Blanco and G. Garcia, Phys. Lett. A **330**, 230 (2004).
[46]A. G. Sanz, M. C. Fuss, F. Blanco, F. Sebastianelli, F. A. Gianturco, and G. Garcia, J. Chem. Phys. **137**, 124103 (2012).
[47]G. Staszewska, D. W. Schwenke, D. Thirumalai, and D. G. Truhlar, Phys. Rev. A **28**, 2740 (1983).
[48]R. Cowan, *The Theory of Atomic Structure and Spectra* (University of California, London, 1981).
[49]M. E. Riley and D. G. Truhlar, J. Chem. Phys. **63**, 2182 (1975).
[50]X. Z. Zhang, J. F. Sun, and Y. F. Liu, J. Phys. B **25**, 1893 (1992).
[51]J. B. Maljkovic, A. R. Milosavljevic, F. Blanco, D. Sevic, G. Garcia, and B. P. Marinkovic, Phys. Rev. A **79**, 052706 (2009).
[52]F. Blanco and G. Garcia, Phys. Lett. A **360**, 707 (2007).
[53]A. Jain, J. Phys. B **21**, 905 (1988).
[54]A. Munoz, J. C. Oller, F. Blanco, J. D. Gorfinkiel, P. Limao-Vieira, and G. Garcia, Phys. Rev. A **76**, 052707 (2007).
[55]Y. Jiang, J. Sun, and L. Wan, Phys. Rev. A **52**, 398 (1995).
[56]T. Yamada, S. Ushiroda, and Y. Kondo, J. Phys. B **41**, 235201 (2008).
[57]D. Shi, J. Sun, Z. Zhu, and Y. Liu, Nucl. Instrum. Methods Phys. B **254**, 205 (2007).
[58]J. A. Beran and L. Kevan, J. Phys. Chem. **73**, 3866 (1969).
[59]Z. Pejcev, M. V. Kurepa, and I. M. Cadez, Chem. Phys. Lett. **63**, 301 (1979).
[60]K. Leiter, P. Scheier, G. Walder, and T. D. Märk, Int. J. Mass Spectrom. Ion Proc. **87**, 209 (1989).
[61]M. Bart, P. W. Harland, J. E. Hudson, and C. Vallance, Phys. Chem. Chem. Phys. **3**, 800 (2001).
[62]B. Sierra, R. Martinez, and F. Castano, Int. J. Mass Spectrom. **225**, 127 (2003).
[63]K. K. Irikura, M. A. Ali, and Y.-K. Kim, Int. J. Mass Spectrom. **222**, 189 (2003).
[64]B. Sierra, R. Martinez, C. Redondo, and F. Castano, Int. J. Mass Spectrom. **235**, 223 (2004).